Nanoscale

PAPER

View Article Online
View Journal | View Issue

Cite this: *Nanoscale*, 2025, **17**, 22334

Unravelling the molecular armor, cellular dynamics and nuclear trafficking of ultra-stable oligopeptylated-AuNPs: PEG-rivalling nanocargos

Salman Khan,[a] Chandra S. Bhatt,[b] Veda V. Dasari[a] and Anil K. Suresh *[a]

Ultra-stable and biocompatible gold nanoparticles (AuNPs) are essential for targeted nanomedicine, facilitating extended circulation, minimal immunogenicity, and efficient cellular uptake. Despite its status as a gold standard for attaining biocompatibility and stability, polyethylene glycol (PEG) faces increasing scrutiny due to its physiology-associated accelerated blood clearance, immunogenicity, and restricted nuclear access, prompting an urgent shift toward alternative surface engineering strategies. This is an extension of our previous study where we fabricated ultra-stable AuNPs using base-etched fish scales, exhibiting PEG-Au comparable physicochemical, mechanical and biofluidic stability. Herein, through integrated surface characterization studies, MALDI-TOF, LC-MS/MS and bioinformatics profiling, we elucidate the shielding oligopeptide consortium that modulates the particles' biomolecular interactions while preserving biofluidic integrity and colloidal stability. Cytotoxicity assays and mechanistic studies of cellular uptake confirmed that the oligopeptylated-AuNPs are non-toxic and are endocytosed *via* clathrin- and scavenger-mediated receptors. Remarkably, ultra-microtome-assisted HR-TEM revealed that our nanocargos could successfully get imported into the nucleus, a rare and highly significant phenomenon, for such non-viral delivery systems. Collectively, our findings position our sustainably bioengineered oligopeptylated-AuNPs as next-generation nanocargos that uniquely integrate biocompatibility, stealth properties and nuclear-targeting capability, offering a versatile and promising platform to enable precision delivery of therapeutic payloads at subcellular resolutions.

Received 5th July 2025,
Accepted 26th August 2025

DOI: 10.1039/d5nr02841h

rsc.li/nanoscale

Introduction

Nanomedicine integrates nanotechnology with theragnostics to enable precise diagnosis and targeted therapy at the molecular level, and has achieved transformative progress by offering diverse nanocarriers that can improve therapeutic payloads, drug solubility, pharmacokinetics, selective targeting and efficiency.[1] By leveraging the large surface area and unique physico-chemical properties, nanomedicines are coming up as next-generation targeted theragnostics by overcoming systemic biological barriers.[2] Since the approval of the first ever nanomedicine, the liposomal doxorubicin (Doxil®) by the Food and Drug Administration (FDA) in 1995, dozens of nanomedicines have translated to the clinic,[3] including combinatorial chemotherapeutics such as Vyxeos® (liposomal cytarabine plus daunorubicin), a siRNA-based nanomedicine Onpattro® (patisiran, a lipid nanoparticle),[4] a lipid-NP mRNA COVID-19 vaccine, *etc.*, to exemplify the potential impact of nanomedicines on health.[5]

Among the diverse nanocarriers, AuNPs are primarily attractive as they are approved by the FDA for clinical use and combine size-tunable opto-electronic properties, inertness, non-immunogenicity and biocompatibility, with ease in their synthesis and surface modifications to engraft diverse targeting moieties.[6,7] However, a persistent challenge with AuNPs is achieving ultrastability, defined as their ability to remain well dispersed in physico-chemical, physiological and biological environments, where biofluids and variable ionic strengths often screen electrostatic repulsion, leading to clumping. For instance, citrate-stabilized AuNPs, although cost-effective and simple to generate, readily aggregate under such treatments,[8] necessitating more robust surface shielding alternatives.

One such widely adopted strategy is polymer encapsulation, with polyethylene glycol (PEG) being the most prevalent and widely recognized gold standard shielding moiety. PEG sterically stabilizes nanoparticles to evade opsonization, offering prolonged systemic circulation.[8] Other significant PEG-like polymers such as poly(vinylpyrrolidone) (PVP) and polyelectrolytes do exist that confer enhanced stability and biocompatibility, even under extreme conditions like high-salt concen-

[a]*Bionanotechnology and Sustainable Laboratory, Department of Biological Sciences, School of Engineering and Sciences, SRM University-AP, Amaravati-522503, India. E-mail: anil.s@srmap.edu.in*
[b]*Departamento de Química Ambiental, Facultad de Ciencias, Universidad Católica de la Santísima Concepción, Concepción, Chile*

trations and freeze–thaw cycles.[6,7] While PEGylation offers notable advantages, it has also sparked considerable controversy, as repeated administration of PEGylated nanocarriers elicits anti-PEG antibodies triggering accelerated blood clearance (ABC), which diminishes therapeutic efficacy and complicates their dosing thresholds.[9] This immune response often stems from complement activation, leading to hypersensitivity, and, in some cases, anaphylaxis.[10] Moreover, even though PEG significantly reduces protein adsorption, it does not entirely prevent it forming a residual protein consortium at high surface PEG densities, which in turn is modulated by PEG chain length and grafting density, influencing cellular uptake, macrophage recognition, and systemic clearance.[11–13] Furthermore, the non-biodegradable nature of PEG raises long-term safety and environmental concerns and repeated exposures have been associated with systemic toxicity and disruption of physiological homeostasis.[9,13] Even under optimized synthesis conditions, PEGylated nanoparticles may aggregate or interact unfavourably with biological membranes, potentially compromising their efficacy and biocompatibility.[13]

Aligned with the quest for intrinsic stability, thiolated small molecules and peptide-based ligands offer a promising bioengineering alternative. These molecules form strong Au–S or Au–N bonds, enhancing colloidal stability and biological stealth.[14,15] In particular, phosphorylated tyrosine (pTyr)-containing peptides exhibit high gold affinity and buffer tolerance, enabling enzyme-responsive behaviour through phosphatase-mediated dephosphorylation, the "phosphate safety lock", to trigger controlled aggregation and release. Such systems illustrate the prominence of the chemical identity of the molecular shield in dictating colloidal stability, drug payload retention, biological interactions, and stimulus-responsive behaviour.[16] The transition towards biomolecular coatings, particularly peptides, represents a paradigm shift in AuNP design, emphasizing multifunctionality, adaptability and biomedical applications.[17–19]

Surface functionalization critically influences the cellular fate and organelle-specific localization of AuNPs, factors that are pivotal in determining their therapeutic efficacy. Ligand-conjugated AuNPs, such as those modified with folic acid or RGD peptides, exploit receptor-mediated endocytosis by cancer cells *via* clathrin- or caveolae-mediated pathways. Folate-AuNPs show efficient lysosomal trafficking in folate receptor-positive cells,[20] while RGD-AuNPs target tumour vasculature through αvβ3 integrin binding.[17] Beyond ligand influence, nanoparticles' morphological and surface characteristics do critically impact their internalization and subcellular routing.[21] Most AuNPs default to endolysosomal localization, which limits therapies requiring cytosolic or nuclear action, necessitating strategic incorporation of nuclear localization signals (NLS) or endosomal escape motifs to enable nuclear targeting.[22,23]

The advancements in surface engineering and intracellular trafficking, though getting expanded towards nuclear targeting, a critical strategy in cancer and gene therapy due to the nucleus's role in regulating DNA-driven processes.[24] However, the nuclear envelope possesses a major hurdle, which permits only particles of sub-10 nm for passive diffusion.[25] Therefore, size control and surface functionalization are the two primary strategies that have been of focus to facilitate nuclear localization of AuNPs. For instance, ultra-small AuNPs between 2 and 6 nm could efficiently penetrate the nuclei of breast cancer cells, whereas AuNPs of over 10 nm remained cytosolic. Notably, 2 nm AuNPs successfully delivered a triplex-forming oligonucleotide, downregulating *c-myc* expression and reducing cell viability.[25] In parallel, biomolecular targeting *via* NLS peptides offered an alternative route to conjugate AuNPs with both the RGD motif (for cellular entry) and SV40 T-antigen-derived NLS efficiently accumulated in the nucleus, disrupting cell division and inducing apoptosis.[26] Targeting intracellular organelles such as the nucleus, mitochondria or lysosomes is critical for minimizing off-target toxicity while achieving spatially controlled drug delivery and enhancing therapeutic efficacy.[27,28] Nuclear delivery is particularly notable for interventions involving DNA damage repair, epigenetic modulation, and gene silencing, which directly influences cellular fate.[29]

Aligned with these principles, we have recently developed a novel class of PEG-mimicking, ultra-stable, and monodisperse AuNPs (~12 ± 4 nm), synthesized through a one-step, sustainable biofabrication route utilizing oligopeptides etched from fish scales.[30] While these particles exhibited outstanding colloidal stability under diverse physicochemical stressors and showed preliminary biocompatibility, the current study extends those findings by addressing critical, unresolved questions pertaining to their biological identity, composition, and intracellular behaviour. Specifically, we investigate the role of endogenous stealth-inducing oligopeptides, their influence on protein adsorption, cytotoxicity profiles, endocytic trafficking routes, intracellular fate, and organelle-specific localization, areas yet unexplored. Using integrated advanced surface characterization studies, MALDI-TOF, LC-MS/MS, and bioinformatics profiling, we elucidate the presence and function of a distinct oligopeptide consortium that shields the AuNPs. These oligopeptides modulate nanoparticle–biomolecule interactions, preserve colloidal stability, and maintain integrity within complex biofluids. Functional assays and mechanistic studies confirm that the oligopeptylated-AuNPs are intrinsically non-toxic and are internalized primarily *via* clathrin- and scavenger receptor-mediated endocytosis. Remarkably, transsectional ultra-microtomy coupled with high-resolution TEM revealed their rare and significant capability to translocate into the nucleus, an attribute with profound implications for non-viral gene and drug delivery. The overall objective of this work is to decipher how the oligopeptylated ultra-stable AuNPs establish a unique molecular "armor" to induce high stability and biocompatibility, govern cellular dynamics, and achieve nuclear trafficking. Collectively, our findings establish a new class of sustainably synthesized, generalized multifunctional AuNPs that inherently combine biocompatibility, stealth properties, and nuclear-targeting potential, offering a versatile and robust platform for targeted subcellular delivery of theragnostic payloads.

2. Materials and methods

2.1. Materials

Fish scales from *Labeo rohita* having an average diameter of ~12–18 mm were brought from a local fish market in Mangalagiri, AP. Auric(III)chloride trihydrate, carboxy poly (ethylene glycol) (cPEG-COOH, average M_n 3500), 3-(4,5-dimethylthiazol-2-yl)-2,5-diphenyltetrazolium bromide (MTT), dithiothreitol (DTT), acrylamide, bisacrylamide, ammonium persulfate, *N*,*N*,*N*′,*N*′-tetramethylethylenediamine, protein ladders, chlorpromazine hydrochloride, dynasore hydrate, cytochalasin D, methyl-β-cyclodextrin and polyinosinic acid were procured from Sigma-Aldrich Ltd, USA. A live/dead staining kit, DMEM cell culture medium, and FBS were purchased from Invitrogen, USA. TEM Grids were purchased from Ted Pella Inc., USA. The rest of the chemicals, solvents, and reagents were from standard commercial sources and of highest quality.

2.2. Synthesis of ultra-stable oligopeptylated-AuNPs

Ultra-stable and biocompatible monodisperse AuNPs were synthesized as reported by us earlier.[30] Briefly, ~70 mg of fish scales (thoroughly cleaned using tap water followed by Milli-Q water) were treated with 4 mL of freshly prepared 4 mM $HAuCl_4$ suspension in a glass vial. The pH was adjusted to 12 using 1 N NaOH, and the mixture was incubated at 90 °C in a dry bath for 6 hours.[30] The synthesis was visually monitored for the colorimetric transition from the yellow hue of the $HAuCl_4$ suspension to a ruby red colour from the AuNPs. The resulting oligopeptylated-AuNPs were subjected to extensive washing *via* centrifugation utilizing Milli-Q water for the identification of stability-inducing surface oligopeptides, and the determination of the cytotoxicity, endocytic pathway, cellular fate and organelle distribution of the as-produced oligopeptylated-AuNPs.

2.3. Isolation of the active oligopeptides responsible for ultra-stability and high dispersity

To identify the active oligopeptides responsible for the high dispersity of the AuNPs, peptide extraction was performed from the AuNPs. Briefly, AuNPs were incubated with 150 mM dithiothreitol (DTT) in 50 mM ammonium bicarbonate buffer at 60 °C for 60 minutes to facilitate the release of surface-bound peptides. After incubation, the mixture was centrifuged at 15 000*g* for 15 minutes to pellet the AuNPs, and the supernatant containing the extracted peptides was carefully collected. The extracted peptides were analyzed using 15% SDS-PAGE under reducing conditions, followed by silver staining to visualize low-abundance peptide species. As controls, protein samples were extracted from fish scales using conventional treatment methods and were processed similarly. Additionally, fish scales incubated at 90 °C and pH 12 in the absence of $HAuCl_4$ were subjected to identical extraction and electrophoresis as comparative controls.

2.4. Identification of the oligopeptides ultra-stabilizing the AuNPs using mass spectrometry

The Au-associated oligopeptides were initially extracted using ammonium acetate-based salting out followed by desalting using spin column filtration. The purified oligopeptides were quantified using a bicinchoninic acid protein assay to ensure appropriate loading for downstream mass spectrometry analysis. Subsequently, LC-MS/MS was performed using a high-resolution Orbitrap mass spectrometer (Thermo Scientific, USA) equipped with a nanospray ionization source. Peptides were separated on an RSLC C18 analytical column (75 μm × 25 cm, 2 μm, 100 Å) maintained at 40 °C using a 60-minute linear gradient with solvent A (0.1% formic acid in water) and solvent B (0.1% formic acid in 80% acetonitrile), with a 2 μL injection volume. MS1 spectra were acquired using an Orbitrap at a resolution of 120 000 over a scan range of *m*/*z* 400–1600 in positive ion mode (spray voltage: 1900 V; ion transfer tube temperature: 275 °C). Data-dependent MS/MS was performed using EThcD fragmentation in the ion trap with quadrupole isolation (0.7 *m*/*z* window), a dynamic exclusion of 45 s, and a mass tolerance of ±10 ppm. Raw data were processed in Proteome Discoverer 3.0 using the Sequest HT algorithm. Database searches were performed against curated FASTA files of *Labeo rohita*, including a contaminant database to eliminate false positives. High-confidence peptide-spectrum matches were filtered using charge-state-dependent XCorr thresholds, and the resulting protein identifications were annotated using integrated functional annotation tools, retaining only master proteins for final reporting.

2.5. Cytotoxicity assessments

The cytotoxicity levels of oligopeptylated-AuNPs were evaluated in HEK 293, HeLa, and RAW 264.7 cell lines separately using MTT assay. Cells were seeded into 96-well plates at an appropriate density and allowed to adhere for 24 hours under standard culture conditions. Following incubation, the cells were gently washed with phosphate-buffered saline (PBS), and complete DMEM (containing 10% FBS) was added. Oligopeptylated-AuNPs were introduced at final concentrations ranging from 50 to 200 μg mL^{-1} and incubated for an additional 24 hours. After that, 20 μL of MTT reagent (5 mg mL^{-1} in PBS) was added to each well and incubated for 4 hours at 37 °C. The resulting formazan crystals were dissolved in 100 μL of dimethyl sulfoxide (DMSO), and the absorbance was measured at 570 nm using a microplate reader. Cell viability was calculated relative to untreated controls, and all experiments were performed in triplicate to ensure reproducibility. Data are expressed as mean values ± standard deviation (SD). Comparisons between groups were assessed using one-way ANOVA followed by Tukey's *post hoc* analysis to determine statistical significance. A *p*-value less than 0.05 was considered indicative of a statistically significant difference.

Cell viability was assessed using the LIVE/DEAD™ Cell Imaging Kit (488/570, Thermo Fisher Scientific) following the manufacturer's instructions. Cells were cultured in appropriate

cell culture vessels suitable for fluorescence microscopy. The Live Green and Dead Red staining reagents were thawed, mixed to prepare a 2× staining solution, and added in equal volumes to the culture medium. After 15 minutes of incubation at 25 °C, the cells were rinsed once in PBS to immediately image them using a fluorescence microscope.

2.6. Quantitative cellular uptake and nuclear localization based on ICP-OES

To quantitate the cellular internalization of oligopeptylated-AuNPs, HeLa and RAW 264.7 cells were seeded into 6-well plates and allowed to adhere for 24 hours as described above. Following this, the cells were treated with oligopeptylated-AuNPs at a concentration of 100 μg mL^{-1} in complete DMEM (10% FBS) and incubated for 24 hours. After incubation, the cells were thoroughly rinsed three times with PBS to remove unbound nanoparticles. The cells were then harvested and digested in freshly prepared aqua regia (nitric acid : hydrochloric acid; 3 : 1 v/v). The resulting digests were diluted to a final volume of 3 mL using a mixture of 2% nitric acid and 1% hydrochloric acid (1 : 1 v/v) before analysis using ICP-OES upon appropriate dilution.

Separate ICP-OES experiments were performed to quantify nuclear internalization of Au by isolating nuclei using a commercial nuclear extraction kit (Sigma-Aldrich, USA), following the manufacturer's protocol. Briefly, treated cells were lysed in lysis buffer using a pestle and mortar for 5 min, followed by centrifugation at 1000*g* for 10 min. The resulting pellet was resuspended in lysis buffer, and nuclei were precipitated with the supplied precipitation buffer. All procedures were performed at 4 °C, handling them rapidly to preserve the nuclear integrity. The isolated nuclei were subsequently digested in aqua regia and analysed by ICP-OES as described above. The percentage of AuNPs localized in the nucleus was determined by quantifying the Au content in isolated nuclei relative to the total Au content analysed in whole cells. The amount of internalized gold was normalized to the number of cells and reported as nanograms per 10^4 cells. Certified gold standard suspensions (0.1, 1, 10, 50, and 100 ppm) were prepared for each experiment as calibrant suspensions.

2.7. Ascertaining the endocytic pathway mechanism

To elucidate the cellular uptake mechanisms of oligopeptylated-AuNPs, HeLa cells were first subjected to MTT assay to evaluate the cytotoxicity of each endocytic inhibitor at various concentrations as described above. Based on these results, the non-toxic concentrations maintaining ≥80% cell viability were selected for performing mechanistic studies. Subsequently, the cells were pre-treated with specific endocytic inhibitors targeting distinct internalization pathways. The cells were incubated for 3 hours at 37 °C with the following inhibitors at their optimized working concentrations: chlorpromazine (CPZ, 10 μg mL^{-1}), methyl-β-cyclodextrin (MβCD, 5 mg mL^{-1}), cytochalasin D (10 μg mL^{-1}), dynasore (80 μM), and polyinosinic acid (PI, 100 μg mL^{-1}). An additional condition at 4 °C was included to assess energy-dependent uptake. Following pre-treatment, the cells were exposed to oligopeptylated-AuNPs (100 μg mL^{-1}) in complete DMEM (cDMEM) for 6 hours. After incubation, the cells were thoroughly washed with PBS to remove non-internalized nanoparticles, harvested, and digested. The intracellular gold content was quantified using ICP-OES to determine the extent of Au uptake under each condition (Fig. 1).

2.8. Endocytic fate and organelle trafficking

Cell pellets at a confluence of 10×10^4 were initially fixed in 2.5% glutaraldehyde prepared in 0.1 M phosphate buffer (pH 7.4) at 4 °C for 1 hour. Post-fixation was performed using 1% osmium tetroxide at 4 °C for 2 hours. The samples were then subjected to a graded ethanol dehydration series (30%, 50%, 70%, 90%, and 100%), followed by treatment with a 1 : 1 mixture of ethanol and acetone. Subsequently, the samples were infiltrated with a 1 : 1 solution of acetone and epoxy resin for 1 hour and embedded in SPI-PON 812 resin, cured at 60 °C for 48 hours. Ultrathin sections (~40 nm) were obtained using a Leica EM UC7 ultramicrotome and stained with uranyl acetate and lead citrate. Imaging of the trans-sectioned specimens was performed on a HRTEM (JEOL, JEM-2100Plus, Japan).

2.9. Instrumentation and material characterization

Solution-phase absorption spectra of the as-is oligopeptylated-AuNP samples were recorded in standard 96-well plates using a Thermo Scientific™ Multiskan™ Sky Spectrophotometer operating at a wavelength resolution of 1 nm. Dynamic light scattering (DLS) and zeta potential (ZP) measurements were performed on a Malvern Instrument (Malvern Instruments, NY, USA). Appropriately diluted 1 mL of AuNPs was used for the DLS and ZP measurements and HRTEM (JEOL, JEM-2100 PLUS, Japan). Peptidaceous functional groups were analyzed using a Bruker Alpha II FTIR spectrometer in the ATR mode. For MALDI-TOF MS, the pristine fish scale protein was prepared by digestion using trypsin with minor modifications, whereas the oligopeptide associated with the AuNPs was extracted using DTT as described in the methods section. 1 μL of the resultant oligopeptide was spotted on a ground steel MTP 384 target plate, air-dried, and overlaid with 1 μL of 0.1 g L^{-1} HCCA matrix and was allowed to dry before performing MALDI TOF MS measurements in the positive mode over a broad *m*/*z* range of 2000–20 000 kDa (ultrafleXtreme, Bruker Daltonics, Bremen, Germany) (Fig. 2).

3. Results and discussion

3.1. Synthesis and characterization of oligopeptylated-AuNPs

The synthesis of ultra-stable and biocompatible oligopeptylated-AuNPs was performed following our previously reported sustainable synthetic route employing fish scale etched oligopeptides as dual reducing and stabilizing agents.[30] The average particle size, as determined from TEM images (n > 100), was ~12 ± 4 nm. HR-TEM images of the oligopeptylated-

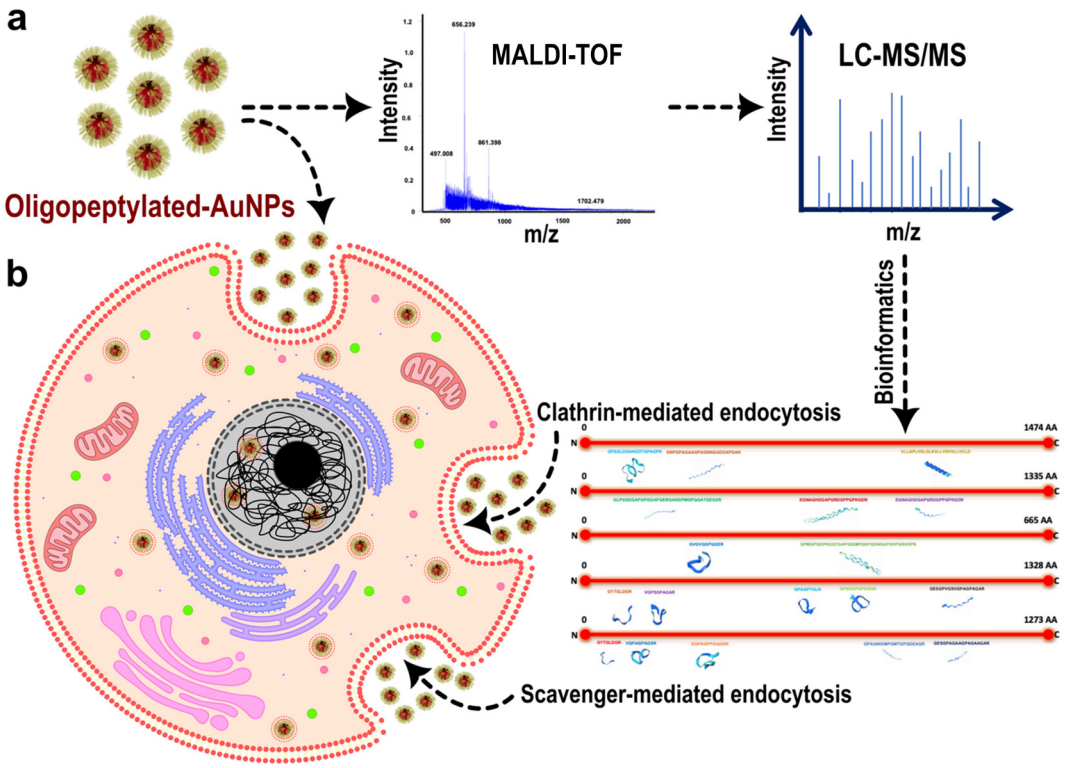

Fig. 1 (a) Schematic representation of the identification of oligopeptides providing intrinsic ultrastability and biocompatibility based on proteomics, mass spectrometry and bioinformatics tools. (b) Cellular toxicity, fate, pathway mechanism and nuclear trafficking of ultra-stable oligopeptylated-AuNPs.

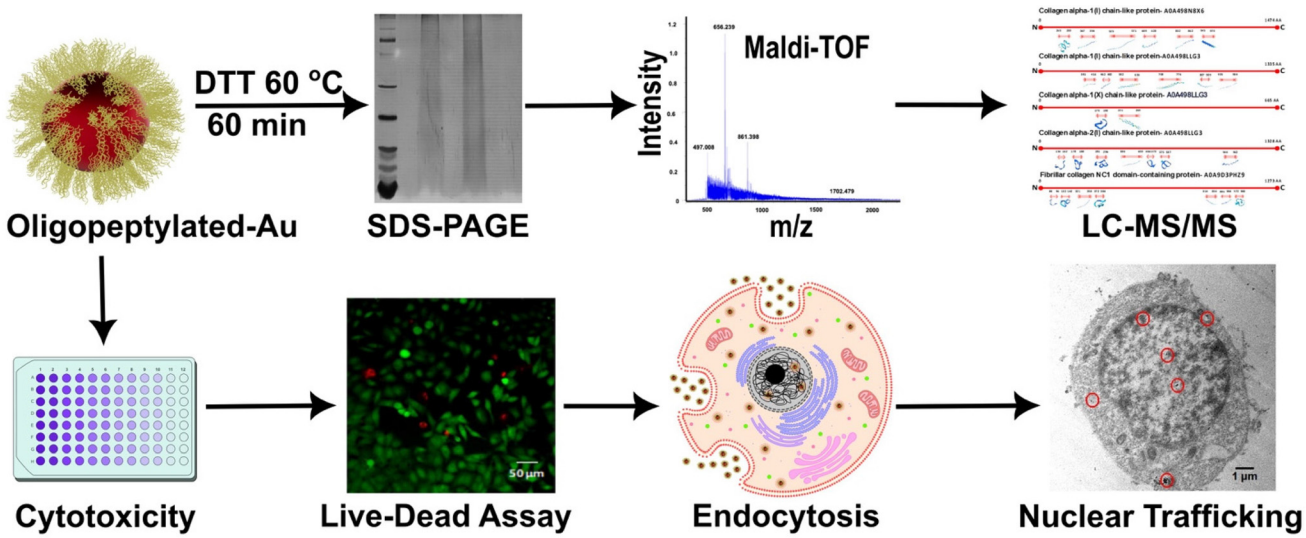

Fig. 2 Stepwise schematic outlines the experimental workflow used to identify the stability-inducing oligopeptides associated with the AuNPs based on downstream biophysical analyses, proteomic profiling, MALDI-TOF and LC-MS/MS and bioinformatics analysis. Following incubation with cells, the resulting oligopeptylated-AuNPs were subjected to cell cytotoxicity assessments, endocytosis pathway analysis, and ultramicrotome transsectioned HRTEM imaging to assess cellular fate and trafficking.

AuNPs captured at progressively higher magnifications revealed uniformly distributed, small spherical nanoparticles ranging from ~10 to 14 nm (Fig. S1a and c). UV–visible spectroscopy confirmed their representative absorbance peak centred around 522 nm, consistent with the formation of well-dispersed, colloidally stable AuNPs (Fig. S1b).

3.2. Isolation of the active oligopeptides responsible for ultra-stability and high dispersity

To elucidate the molecular determinants responsible for inducing ultrastability and biocompatibility to the oligopeptylated-AuNPs, we systematically investigated their surface-bound oligopeptide consortium. The Au surface stabilizing oligopeptides were extracted by treating the AuNPs with 150 mM dithiothreitol in ammonium bicarbonate buffer (50 mM, pH 8.0), a condition optimized to cleave disulfide bonds and disrupt gold–thiol interactions, thereby releasing the covalently linked oligopeptides. This method is analogous to previously reported strategies for desorbing thiolated ligands and peptides from the surface of noble metal nanoparticles *via* reductive displacement.[31,32] Comparative controls were established to assess the specificity and origin of the stabilizing biomolecules and included (i) crude or pristine fish scale proteins extracted using standardized procedures and (ii) fish scale proteins subjected to reaction identical alkaline hydrothermal treatment (pH 12, 90 °C) without the addition of a gold precursor. SDS-PAGE analysis followed by silver staining revealed a markedly smeared banding pattern for oligopeptylated-AuNP samples, indicative of heterogeneous low molecular weight peptide fragments. In contrast, pristine fish scale proteins yielded distinct, well-resolved bands corresponding to native, intact collagenous and non-collagenous proteins (Fig. 3a). On the other hand, the thermally treated fish scales in the absence of the Au precursor displayed a similar smear to that of oligopeptylated-AuNPs, suggesting significant hydrolysis and peptide fragmentation due to the alkaline heat treatment, a phenomenon well documented in collagen degradation kinetics under denaturing conditions (Fig. 3b).[33]

To further characterize the molecular identity of the surface-bound oligopeptides, matrix-assisted laser desorption/ionization time-of-flight mass spectrometry (MALDI-TOF MS) was performed. The AuNP extracted oligopeptides displayed characteristic mass peaks in the range of 497–861 Da (Fig. 3e), consistent with oligopeptide profiles. The use of such oligopeptides as natural "molecular shields" echoes recent findings in bioinspired nanomaterials, where peptides derived from degraded extracellular matrix proteins or engineered short sequences have been shown to stabilize Au nanostructures in

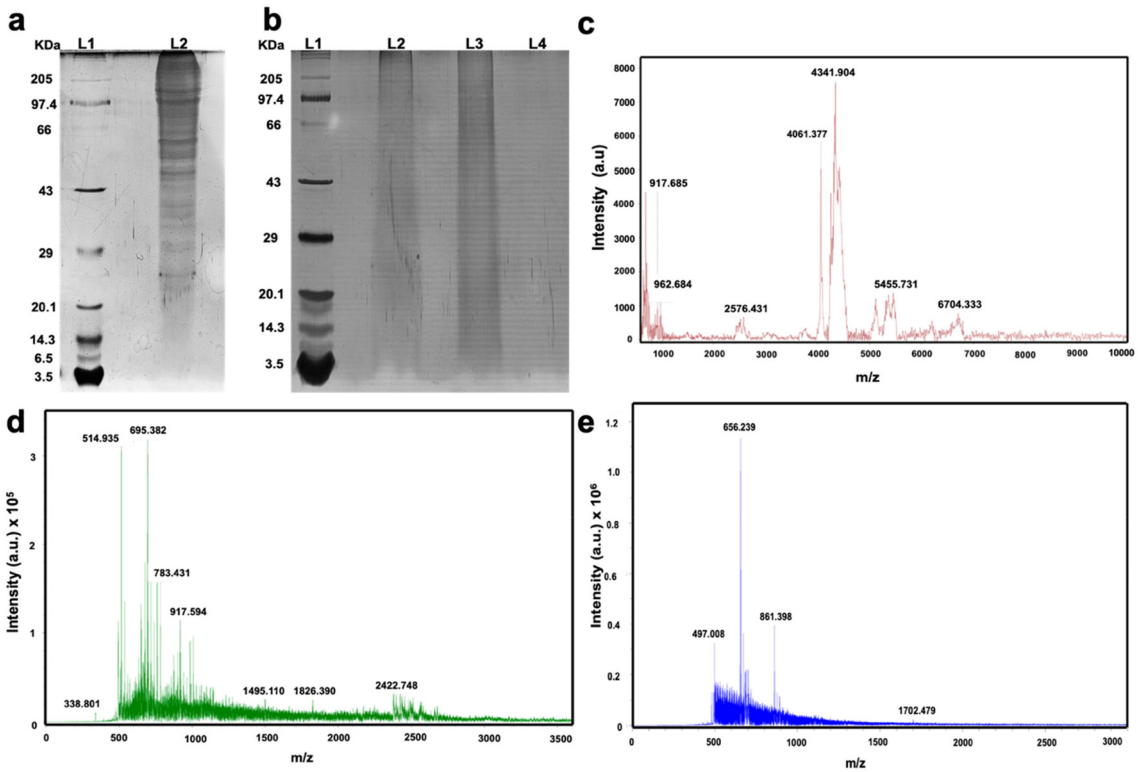

Fig. 3 (a and b) SDS-PAGE upon silver staining: lane 1 (L1) in (a) and (b) is the protein marker and lane 2 (L2) in (a) shows pristine fish scale proteins (controls) exhibiting well-resolved high molecular weight bands and L2 in (b) shows a distinct smeared band pattern in the peptide extract from oligopeptylated-AuNPs, indicating the presence of heterogeneous low-molecular-weight peptides, while lane 3 (L3) shows thermally treated fish scale proteins (without Au precursor) displaying a similar smear to that of oligopeptylated-AuNPs, suggesting heat and alkaline-induced proteolysis. (c) MALDI-TOF spectrum of pristine fish scale proteins reveals high molecular weight peaks in the range of 2576–6700 Da, corresponding to intact protein domains. (d) MALDI-TOF profile of thermally treated fish scale proteins without gold and for the peptides desorbed from oligopeptylated-AuNPs shows dominant peaks between 500 and 1000 Da, consistent with short oligopeptides. The striking similarity between spectra (d) and (e) supports the hypothesis that alkaline-thermal hydrolysis liberates amphiphilic peptide fragments that bind to AuNP surfaces, forming a natural "molecular shield" that confers colloidal stability and biocompatibility.

physiological medium.[34,35] Contrarily, pristine scale proteins revealed higher molecular weight peptides (2576–6700 Da), consistent with longer intact polypeptide chains and folded protein domains (Fig. 3c). Importantly, alkaline-thermal treated scales without Au yielded oligopeptide profiles closely resembling oligopeptylated-AuNPs, falling within the range of 514–900 Da (Fig. 3d). This similarity supports the hypothesis that the AuNP synthesis environment promotes controlled proteolysis, liberating short amphiphilic peptide fragments that subsequently act as stabilizing moieties for the *in situ* formation of AuNPs. These peptides likely get adsorb onto the nanoparticle surface *via* multidentate interactions, thereby forming a compact biomolecular coat providing colloidal stability, resistance to aggregation in biological fluids and non-specific molecular interactions *in vivo*.[36–38]

This unique "molecular shield" strategy, wherein endogenous oligopeptides serve as dual reducing and stabilizing agents, offers a biologically derived sustainable alternative to synthetic PEG encapsulation, avoiding immunogenicity and complement activation risks associated with PEG.[39] Meritoriously, the presence of peptide ligands also offers functional advantages: their amphiphilic nature facilitates cellular uptake, and sequence composition could potentially be tailored for organelle targeting, including the nucleus, as observed in arginine-rich or nuclear localization signal (NLS)-bearing sequences.[40] Taken together, our findings point towards a unique biomolecular engraftment composed of fragmented oligopeptides that confer exceptional dispersity, biocompatibility, and stability to oligopeptylated-AuNPs, supporting their potential for targeted intracellular delivery and nuclear trafficking.

3.3. Identification of the oligopeptides associated with the AuNPs using LC-MS/MS and bioinformatics

To investigate the molecular basis of the exceptional colloidal and biological stability of the oligopeptylated-AuNPs, we conducted detailed proteomic analysis of surface-bound biomolecules using LC-MS/MS following reductive desorption. Fish scales, the parent biomaterial, are known to be rich in extracellular matrix (ECM) proteins, particularly type I collagen, which comprises 40–70% of total protein content on a dry weight basis depending on species and extraction conditions.[41] These structural proteins are characterized by a high abundance of glycine (13–16%), proline, hydroxyproline, arginine, and serine—residues essential not only for collagen's structural stability but also for their potential interactions with metal surfaces.[42] The reductively released biomolecular consortium from oligopeptylated-AuNPs was subjected to LC-MS/MS, revealing 28 unique peptides (Table S1), predominantly derived from collagen alpha-chain isoforms, including type I, type X, and NC1 domains containing fibrillar collagen-like proteins (Fig. 4a).

The oligopeptides ranged in their lengths composed of 8 to 68 amino acids and exhibited sequence motifs characteristic of ECM proteins, notably the repeating Gly–Pro–X (GPX) motif, where X was often a polar or charged amino acid such as glutamic acid (E), serine (S), or alanine (A). This GPX motif is fundamental to the triple-helix structure of collagen and is widely recognized for imparting protease resistance, thermal stability, and low immunogenicity, desirable for prolonged systemic circulation and cellular interface applications.[43] The enrichment of collagen-mimetic domains suggests that the surface of oligopeptylated-AuNPs is coated with biocompatible and functionally competent ECM-like peptides, capable of engaging integrins or matrix receptors, thus potentially aiding in cellular adhesion, signalling, and uptake.[44,45]

Notably, the GRAVY (Grand Average of Hydropathy) scores calculated for the identified peptides revealed predominantly negative values, indicating strong hydrophilicity (Fig. 4b). Oligopeptides such as EGPAGPPGQDGR (GRAVY: −1.633) and GPSGSPGPDGNK (GRAVY: −1.575) are exemplary in promoting

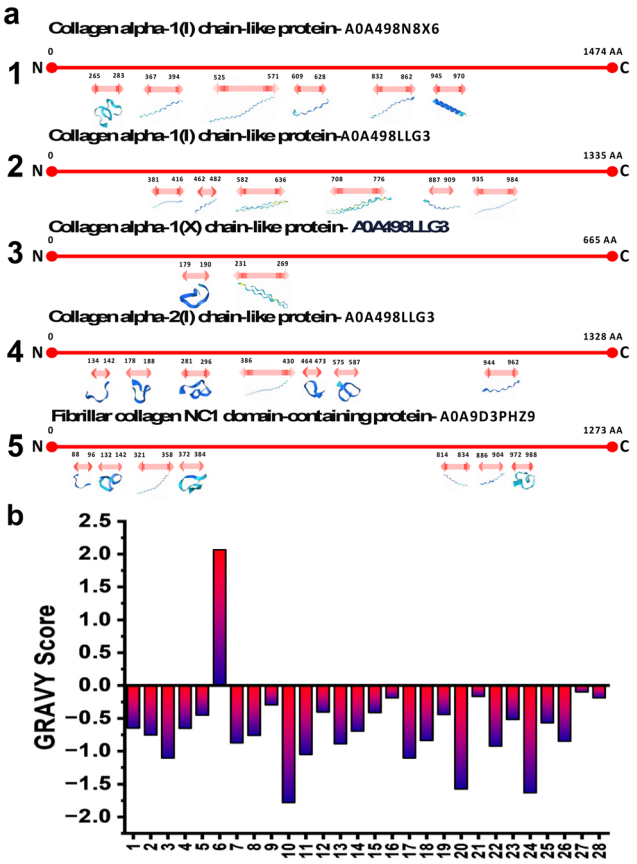

Fig. 4 (a) Proteomic profiling and sequence analysis of the peptide consortium of oligopeptylated-AuNPs. Domain mapping of peptides identified from LC-MS/MS analysis, matched against various collagen isoforms: (1) collagen alpha-1(I) chain-like protein, (2) collagen alpha-1(I) chain-like protein (alternate isoform), (3) collagen alpha-1(X) chain-like protein, (4) collagen alpha-2(I) chain-like protein, and (5) fibrillar collagen NC1 domain-containing protein. Peptide fragments (shown as horizontal arrows) span multiple structural domains including triple-helical regions and non-collagenous terminal segments, suggesting broad proteolytic fragmentation of extracellular matrix components during nanoparticle synthesis. (b) GRAVY (Grand Average of Hydropathy) scores of identified peptides from oligopeptylated-AuNPs, highlighting predominantly negative values indicative of strong hydrophilicity.

hydration shell formation around the NPs, thereby enhancing dispersion stability in aqueous and physiological media. Hydration layers mediated by polar and hydrogen-bonding residues are known to provide steric stabilization by repelling close particle–particle interactions, a mechanism functionally analogous to PEGylation but devoid of immunogenic risks.[46] In addition to hydration-based stabilization, the oligopeptides displayed high contents of charged and polar residues, particularly aspartic acid (D), glutamic acid (E), serine (S), threonine (T), and arginine (R). These residues confer electrostatic stabilization *via* surface charge repulsion, critical for preventing NP aggregation in ionic environments such as blood plasma. Such electrostatic and hydration-derived forces represent a dual mechanism of colloidal stability, effectively replacing synthetic polymeric stabilizers.

Importantly, the presence of ECM-like peptide motifs may play a role not only in colloidal stability but also in modulating biological fate. Short collagen-derived peptides and motifs such as RGD and GFOGER have been shown to interact with integrin receptors, facilitating receptor-mediated endocytosis.[47,48] The dense peptide coating on oligopeptylated-AuNPs, rich in ECM-associated sequences, may thereby support efficient uptake by target cells *via* integrin engagement or matrix-mimetic interactions, a process reported to enhance endosomal escape and, in certain cases, nuclear localization depending on the peptide architecture and charge. Collectively, the proteomic evidence reveals that oligopeptylated-AuNPs are cloaked with sophisticated, multifunctional peptides derived from thermally fragmented fish scale collagen. These peptides offer a "natural molecular shield" that simultaneously confers aqueous stability, resists nonspecific protein adsorption, and potentially mediates specific biological interactions. By substituting synthetic PEG with endogenous peptide ligands, these nanoparticles not only maintain colloidal integrity but also possess the biomimetic versatility necessary for controlled cellular uptake and intracellular trafficking, including nuclear delivery, aligning with the strategic goals of next-generation nanomedicines.

3.4. Cytocompatibility assessment of the oligopeptylated-AuNPs

The biocompatibility of oligopeptylated-AuNPs was assessed based on MTT assay (Fig. 5a) and live/dead fluorescence staining (Fig. 5d–i) in three representative mammalian cell lines: HeLa, RAW 264.7, and HEK 293. Across all cell types and concentrations (up to 200 μg mL^{-1}), oligopeptylated-AuNPs exhibited minimal cytotoxicity, maintaining >85–90% viability in c-DMEM, consistent with nanomaterials possessing biologically derived surface coatings.[49] Live/dead imaging corroborated these findings, with predominant green fluorescence indicating intact membranes and low apoptosis, even under high dosage.

Importantly, the absence of significant cytotoxicity in RAW 264.7 cells, a phagocytic and immunologically sensitive line, suggests a low immunogenic and pro-inflammatory profile. This is particularly notable given that macrophages readily internalize foreign particles and are often early indicators of nanoparticle-associated stress.[50] Collectively, these results validate that oligopeptylated-AuNPs are highly cell-compatible, offering a stable and non-toxic platform for subsequent investigations into intracellular trafficking, endocytic routing, and nuclear delivery.

3.5. Quantitative cellular uptake and nuclear localization of oligopeptylated-AuNPs

Quantitative cellular uptake measurements based on ICP-OES revealed time-dependent internalization of oligopeptylated-AuNPs in both HeLa (non-phagocytic) and RAW 264.7 (phagocytic) cell lines, with the uptake increasing over 1–24 h in both serum-free DMEM (synthetic identity) and serum-supplemented DMEM (biological identity) (Fig. 5b and c). Notably, higher intracellular accumulation was consistently observed in synthetic identity compared to biological identity across all time points in both cell types. In HeLa cells, the uptake increased from 39.2 ng per 10^6 cells at 1 h to 730.1 ng per 10^6 cells at 24 h in synthetic identity, *versus* 27.2 to 587.0 ng per 10^6 cells in biological identity. Similarly, RAW 264.7 macrophages showed a more pronounced uptake, reaching 1207.8 ng per 10^6 cells at 24 h in synthetic identity, compared to 1085.8 ng per 10^6 cells in biological identity. These findings underscore that serum proteins modulate nanoparticle–cell interactions, likely through the formation of a biomolecular corona that masks surface ligands or alters the physicochemical identity of the particles, thus lowering the uptake rates, a phenomenon widely reported for gold and other nanoparticles.[51,52]

Interestingly, oligopeptylated-AuNPs maintained high colloidal stability and active internalization in both media. This can be attributed to natural oligopeptides, derived from collagen-rich fish scale proteins, which offers hydration shell-mediated steric repulsion and electrostatic stabilization without interfering with receptor-mediated or adsorptive uptake.[44,45] The more efficient uptake in synthetic identity may be due to greater exposure of the peptide-rich surface, promoting interactions with negatively charged cell membranes *via* hydrogen bonding or electrostatic attraction.[53]

RAW 264.7 macrophage cells exhibited overall higher internalization than HeLa cells, which is consistent with their phagocytic nature and enhanced endocytic activity.[54] However, the difference between synthetic identity and biological identity remained evident, suggesting that even phagocytic uptake is influenced by media-induced changes in nanoparticle identity. These results not only confirm that oligopeptylated-AuNPs retain functional biointerfaces even in protein-rich biological fluids, but also highlight the importance of media composition in dictating nanoparticle uptake and downstream intracellular fate. The robustness of cellular internalization in both environments, especially in immune and epithelial cancer cells, supports the potential of oligopeptylated-AuNPs as PEG-free, bio-inspired delivery platforms for targeted therapeutic or nuclear localization applications.

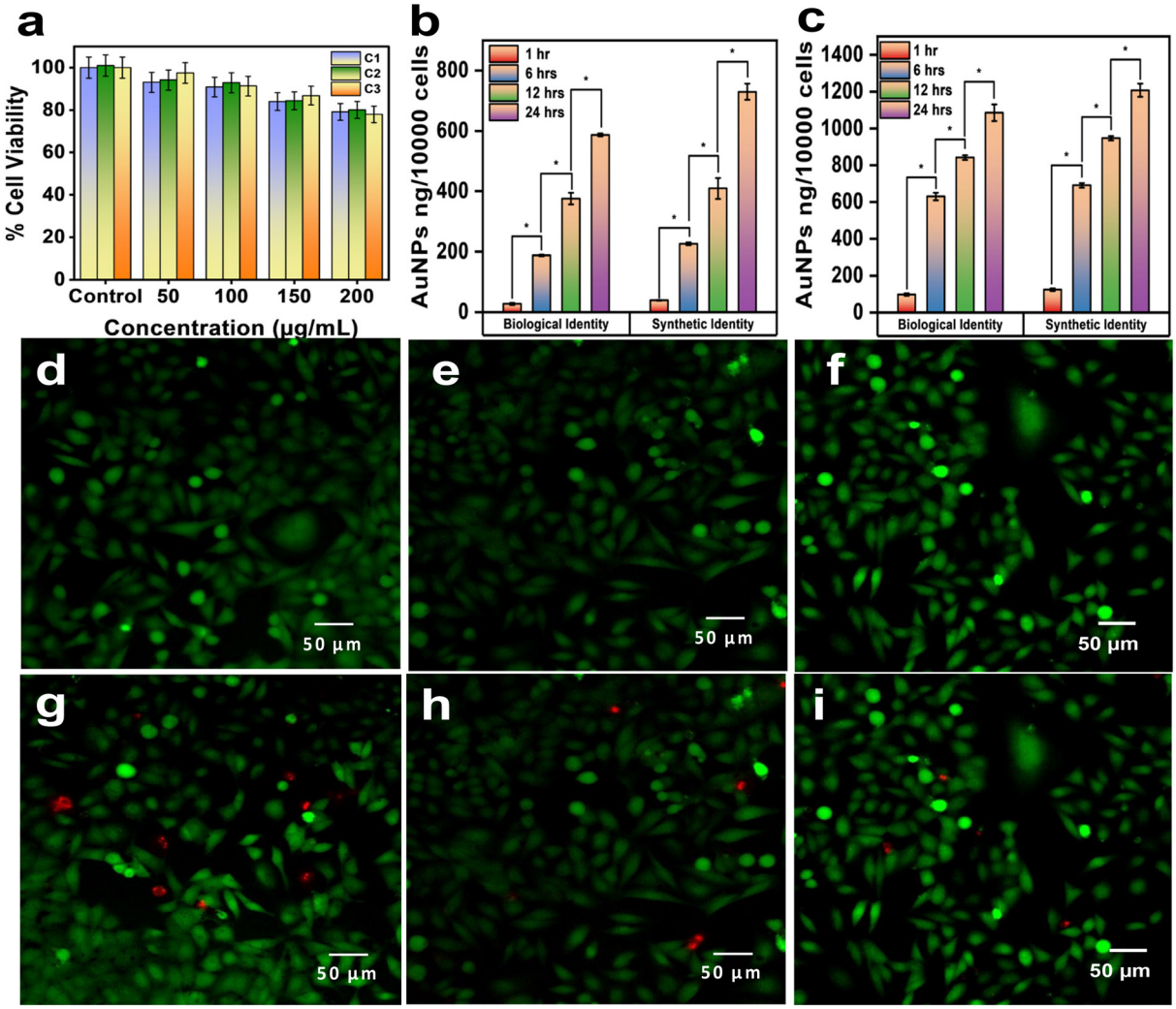

Fig. 5 Cytocompatibility and cellular uptake efficiency of oligopeptylated-AuNPs. (a) MTT assay showing the percentage cell viability of (C1) HeLa cells and (C2) RAW 264.7 macrophages and (C3) HEK 293 cells after 24 h treatment with varying concentrations (10–200 μg mL^{-1}) of oligopeptylated-AuNPs in cDMEM. (d) Live/dead staining of HeLa cells and (h) RAW 264.7 cells and (i) HEK 293 exposed to oligopeptylated-AuNPs (100 μg mL^{-1}), indicating predominant green fluorescence (live cells) with minimal red staining (dead cells), confirming negligible cytotoxicity; and (d–e–f) controls of the respective cells. Quantitative analysis of oligopeptylated-AuNP internalization in (b) HeLa (non-phagocytic) and (c) RAW 264.7 (phagocytic) cells over 1, 6, 12, and 24 hours as measured by ICP-OES.

3.6. Endocytic pathway analysis

To decipher the cellular internalization mechanisms of oligopeptylated-AuNPs in synthetic and biological identities, a series of endocytic pathway inhibition studies were performed in HeLa cells using specific chemical inhibitors. To ensure that the observed reductions in uptake were due to specific pathway inhibition and cell viability, we performed MTT assays for each inhibitor at the respective working concentrations (Fig. S2a, b and Table 1, Table S2) and inferred that all inhibitors maintained cell viability of above 80%. These findings corroborate the suitability of these concentrations for mechanistic studies and validate that the inhibition effects reflect genuine pathway suppression rather than off-target cytotoxicity.

Table 1 Comparative physicochemical and biological characteristics of oligopeptylated-AuNPs in synthetic and biological identities

Parameter	Synthetic identity	Biological identity
Hydrodynamic size (nm)	38.45	56.45
Zeta potential (mV)	−20	−29.4
Endocytic pathway	Dynamin-dependent uptake	Clathrin-mediated and scavenger receptor-mediated uptake
Cellular localization	Nucleus and cytoplasm	Nucleus and cytoplasm

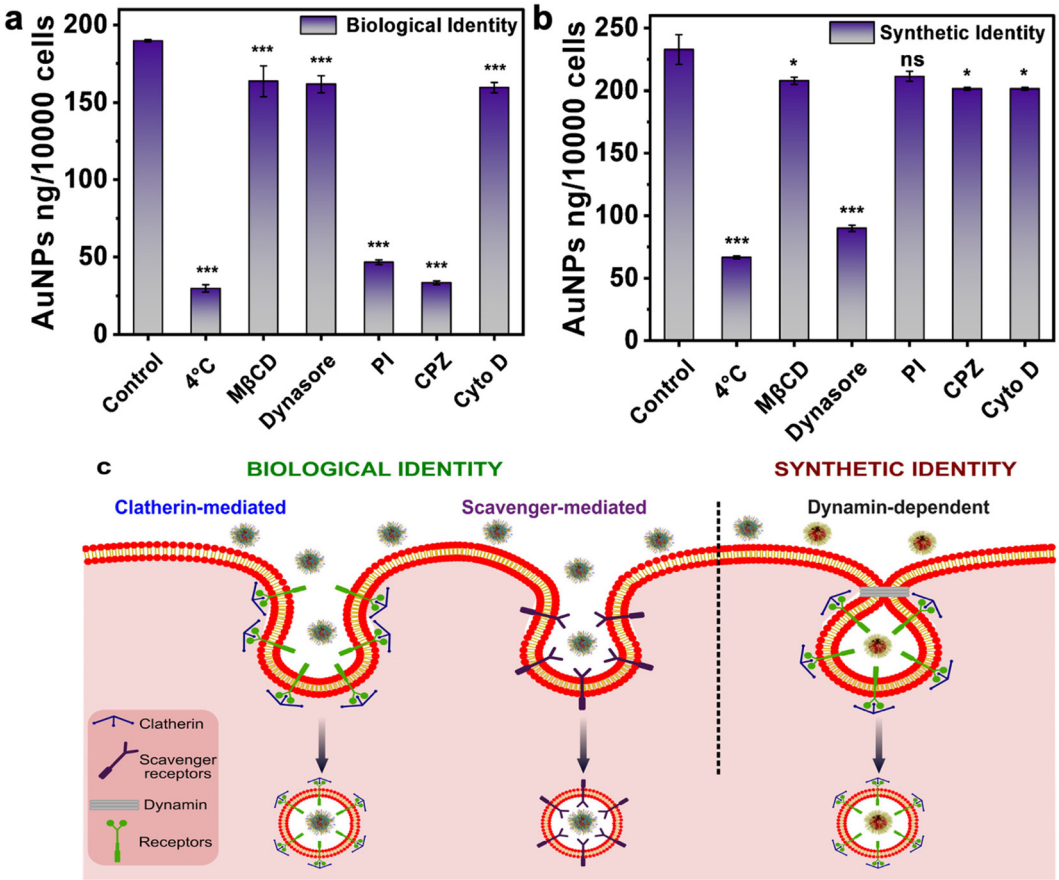

Fig. 6 Endocytic pathway determination for oligopeptylated-AuNPs using inhibitors in HeLa cells. Cells were pre-treated with pathway-specific inhibitors: chlorpromazine (clathrin-mediated), dynasore (dynamin-dependent), cytochalasin D (macropinocytosis), methyl-β-cyclodextrin (lipid raft-/caveolae-mediated), and polyinosinic acid (scavenger receptor-mediated), followed by incubation with oligopeptylated-AuNPs under (a) biological identity (serum supplemented) and (b) synthetic identity (serum-free) conditions. (c) Schematic illustration of internalization pathways of oligopeptylated-AuNPs following clathrin- and scavenger-mediated endocytosis in biological identity and dynamin-dependent endocytosis in synthetic identity.

The cellular uptake (Fig. 6a and b) demonstrates a significant reduction in internalization at 4 °C, confirming the energy-dependent nature of oligopeptylated-AuNPs taken up in both biological and synthetic states. Among the pharmacological inhibitors tested, chlorpromazine (CPZ) and polyinosinic acid (PI) notably suppressed the uptake of oligopeptylated-AuNPs in biological identity, implicating clathrin-mediated endocytosis (CME) and scavenger receptor-mediated uptake as the dominant routes. This behaviour is consistent with earlier reports that serum components often favour receptor-mediated endocytosis *via* opsonins and apolipoproteins that interact with scavenger- and clathrin-associated receptors.[55,56] In contrast, under synthetic conditions, dynasore treatment led to the most substantial inhibition, suggesting a dynamin-dependent endocytic mechanism as the primary route. This shift in uptake mode can be attributed to the altered surface chemistry and lack of serum-derived biological ligands, which may otherwise engage specific membrane receptors.[57] Interestingly, methyl-β-cyclodextrin (MβCD) and cytochalasin D showed only moderate inhibitory effects under both conditions, indicating that lipid raft-mediated and macropinocytotic pathways might contribute minimally to oligopeptylated-AuNP uptake. This suggests that while these pathways remain accessible, they are not the major internalization routes for these ultra-stable AuNPs.

3.7. Transmission electron microscopy unveils nuclear trafficking

We also performed TEM imaging to provide deeper insights into the intracellular fate, distribution and trafficking. Ultrasmall nanoparticles in particular are critical to determine the cellular fate and trafficking, as sub-20 nm particles, due to their ability to traverse endosomal barriers and interact favourably with nuclear pore complexes.[58–60] When we examined the HeLa cells post-incubated with oligopeptylated-AuNPs using TEM imaging a clear piece of evidence of nanoparticle internalization was observed, both in biological identity (Fig. 7a–d) and in synthetic identity (Fig. 7e–h and Table 1). Higher magnification imaging revealed that nanoparticles were consist-

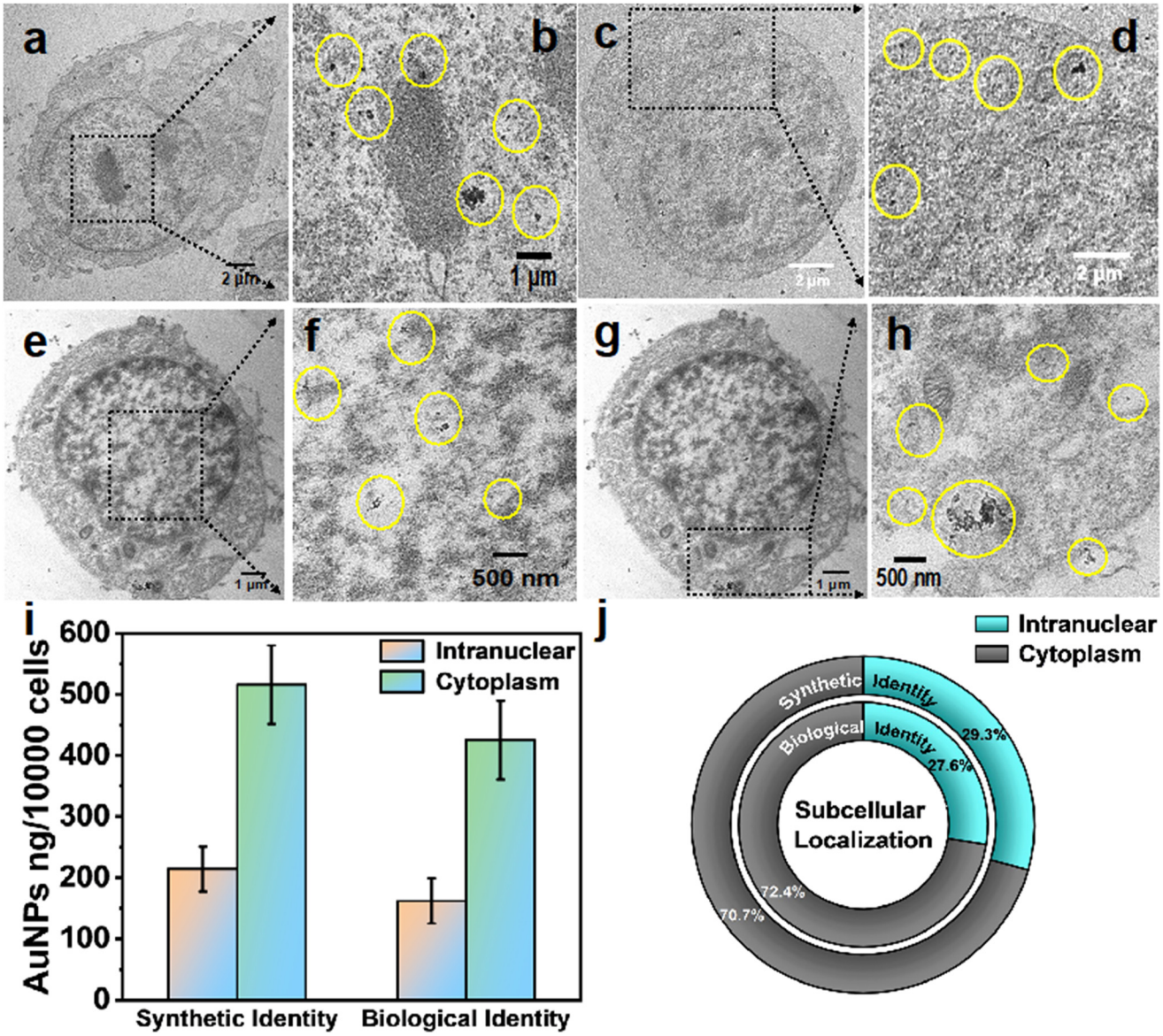

Fig. 7 Transmission electron microscopy (TEM) and ICP-OES analysis of subcellular localization and quantification of oligopeptylated-AuNPs under biological and synthetic identity conditions. TEM micrographs of HeLa cells incubated with oligopeptylated-AuNPs in serum-supplemented medium (biological identity; nucleus (a and b) and cytoplasm (c and d)) and serum-free medium (synthetic identity; nucleus (e and f) and cytoplasm (g and h)) showing intracellular distribution patterns (as indicated by yellow circles). (i) ICP-OES quantification of the uptake of AuNPs by the nucleus and cytoplasm. (j) Pie-chart representation of the sub-cellular relative percentage localization of the AuNPs calculated using ImageJ from the various HR-TEM micrographs captured across various cells on the grid.

ently visualized in the cytoplasmic region enclosed within vesicular structures suggestive of endosomal trafficking.

Strikingly, multiple HR-TEM images captured across multiple cells from diverse grid regions showed Au nanoparticles in close proximity to the nuclear envelope and within the nucleoplasm under both conditions, indicating successful nuclear trafficking, a rare and highly significant phenomenon, for non-viral delivery systems (Fig. 7j). Nuclear targeting of Au by the cells is further supported based on quantitative ICP-OES analysis, by extracting the nucleus, revealing 214.2 ng per 10^6 for cells in synthetic identity and 162.0 ng per 10^6 cells in biological identity (Fig. 7i) compared to the total Au content of 730.1 ng per 10^6 for cells in synthetic identity and 587.0 ng per 10^6 cells in biological identity (Fig. 5b). The comparable ultrastructural distribution under both biological and synthetic identity conditions suggests that the intrinsic properties of oligopeptylated-AuNPs, particularly their ultra-small size, their biogenic surface chemistry, and the likely presence of nuclear-penetrating oligopeptides from fish-scales, facilitate a robust internalization and trafficking pathway, independent of the specific biological identity conferred by serum proteins.

Moreover, achieving nuclear targeting is considered extremely imperative as it enhances the therapeutic efficacy, enables gene editing, improves treatment outcomes, and reduces off-target effects, making it a powerful strategy in nanomedicine.[24] Besides, fabrication of AuNPs that can be trafficked into the nucleus is extremely challenging due to size restrictions of nuclear pores, endosomal entrapment, and endosomal escape,[61,62] whereas our oligopeptylated-Au could surpass the nuclear barrier with utmost ease, presumably due to their small size and GPX-rich oligopeptide surface motifs.[63,64] Finally, we have ongoing *in vitro* cellular fate and *in vivo* systemic biodistribution experiments of our exscalar AuNPs aimed at mapping their organ-level distribution, circulation half-life, and immunogenic response, with a focus on evaluating complement activation, cytokine release, and immune cell engagement, so as to establish a detailed understanding of their safety, stealth properties, and translational potential as next-generation nanocargos.

4. Conclusion

In this continuation study, we comprehensively elucidated the molecular shield, cellular dynamics, and endocytic nuclear trafficking of oligopeptylated ultra-stable gold nanoparticles (AuNPs) derived from acid-etched fish scales. Our findings reveal that the naturally grafted oligopeptide corona not only confers biofluidic and colloidal stability that is comparable to its PEGylated counterparts but also imparts stealth-like functionality and facilitates efficient intracellular delivery. The oligopeptylated-AuNPs exhibited non-cytotoxic behaviour, were internalized predominantly *via* clathrin- and scavenger receptor-mediated endocytosis, and notably achieved nuclear localization while retaining structural integrity—an uncommon feature for non-viral nanocarriers. These attributes collectively position oligopeptylated-AuNPs as a sustainable, biocompatible, and nucleus-targeting alternative to conventional PEG-based platforms. Our results underscore the potential of leveraging bioengineered peptidic interfaces to develop next-generation nanocargos for targeted therapeutic delivery and precision nanomedicine.

Author contributions

Anil K. Suresh: conceived the idea; conceptualized, planned and designed the research and experiments; analyzed and interpreted the results; wrote the manuscript; and performed funding acquisition, project administration, and supervision; Salman Khan: performed all the experiments and characterization studies, analyzed and interpreted the data, managed the outsourced work, and prepared the images and tables for the MS and assisted in writing the MS. Chandra S. Bhatt: assisted the first author in performing all the experiments as well as their optimizations. Veda V. Dasari: prepared the illustrative figures.

Conflicts of interest

The authors declare no conflict of interest.

Data availability

All data supporting the findings of this study are included within the article and its SI. Raw data files from MALDI-TOF, LC-MS/MS, cytotoxicity assays, and HR-TEM imaging are available from the corresponding author upon reasonable request. Bioinformatics scripts and processed datasets used for peptide profiling and molecular interaction analyses are also available upon request to facilitate reproducibility.

Morphological Characterization of the oligopeptylated AuNPs. List of oligopeptides identified from the surface of oligopeptylated-AuNPs by LC-MS/MS. List of endocytic pathway inhibitors to dissect the endocytic pathways involved in oligopeptylated-AuNP. MTT assay evaluating the cytotoxicity of endocytic pathway inhibitors in HeLa cells. See DOI: **https://doi.org/10.1039/d5nr02841h**.

Acknowledgements

A. K. S. thanks the DBT, Government of India, for financial support through the prestigious Ramalingaswami Fellowship Award. A. K. S. also thanks the DBT-ATGC, Government of India, for financial support through Grant No. BT/PR42263/PBD/26/831/2022. The authors thank SCIF and NRC, SRMIST, Chennai, and the DBT-SAHAJ National Facility for Mass Spectrometry at RGCB for instrument characterization.

References

1 Y. Jia, Y. Jiang, Y. He, W. Zhang, J. Zou, K. T. Magar, H. Boucetta, C. Teng and W. He, Approved Nanomedicine against Diseases, *Pharmaceutics*, 2023, **15**(3), 774, DOI: **10.3390/pharmaceutics15030774**.

2 C. L. Ventola, The Nanomedicine Revolution, *Pharmacol. Ther.*, 2012, **37**(9), 512–525.

3 S. Ahmad, R. A. M. Idris, W. N. Wan Hanaffi, K. Perumal, J. C. Boer, M. Plebanski, J. Jaafar, J. K. Lim and R. Mohamud, Cancer Nanomedicine and Immune System—Interactions and Challenges, *Front. Nanotechnol.*, 2021, **3**, DOI: **10.3389/fnano.2021.681305**.

4 T. Lammers and M. Ferrari, The Success of Nanomedicine, *Nano Today*, 2020, **31**, 100853, DOI: **10.1016/j.nantod.2020.100853**.

5 R. Tenchov, R. Bird, A. E. Curtze and Q. Zhou, Lipid Nanoparticles–From Liposomes to mRNA Vaccine Delivery, a Landscape of Research Diversity and Advancement, *ACS Nano*, 2021, **15**(11), 16982–17015, DOI: **10.1021/acsnano.1c04996**.

6 M. A. Dheyab, A. A. Aziz, P. Moradi Khaniabadi, M. S. Jameel, N. Oladzadabbasabadi, S. A. Mohammed,

R. S. Abdullah and B. Mehrdel, Monodisperse Gold Nanoparticles: A Review on Synthesis and Their Application in Modern Medicine, *Int. J. Mol. Sci.*, 2022, **23**(13), 7400, DOI: **10.3390/ijms23137400**.

7 A. M. Alkilany and C. J. Murphy, Toxicity and Cellular Uptake of Gold Nanoparticles: What We Have Learned so Far?, *J. Nanopart. Res.*, 2010, **12**(7), 2313–2333, DOI: **10.1007/s11051-010-9911-8**.

8 J. S. Suk, Q. Xu, N. Kim, J. Hanes and L. M. Ensign, PEGylation as a Strategy for Improving Nanoparticle-Based Drug and Gene Delivery, *Adv. Drug Delivery Rev.*, 2016, **99**, 28–51, DOI: **10.1016/j.addr.2015.09.012**.

9 H. Y. Nguyenova, M. Hubalek Kalbacova, M. Dendisova, M. Sikorova, J. Jarolimkova, Z. Kolska, L. Ulrychova, J. Weber and A. Reznickova, Stability and Biological Response of PEGylated Gold Nanoparticles, *Heliyon*, 2024, **10**(9), e30601, DOI: **10.1016/j.heliyon.2024.e30601**.

10 E. Okła, S. Michlewska, A. Buczkowski, S. Zawadzki, K. Miłowska, J. Sánchez-Nieves, R. Gómez, F. J. de la Mata, M. Bryszewska, J. Blasiak and M. Ionov, Pegylated Gold Nanoparticles Interact with Lipid Bilayer and Human Serum Albumin and Transferrin, *Sci. Rep.*, 2024, **14**(1), 24408, DOI: **10.1038/s41598-024-74898-0**.

11 H. Chen, H. Paholak, M. Ito, K. Sansanaphongpricha, W. Qian, Y. Che and D. Sun, "Living" PEGylation on Gold Nanoparticles to Optimize Cancer Cell Uptake by Controlling Targeting Ligand and Charge Densities, *Nanotechnology*, 2013, **24**(35), 355101, DOI: **10.1088/0957-4484/24/35/355101**.

12 M. M. Garrigós, F. A. de Oliveira, C. J. S. Costa, L. R. Rodrigues, M. P. Nucci, A. d. H. Alves, J. B. Mamani, G. N. d. A. Rego, J. M. Munoz and L. F. Gamarra, Assessing the Toxicity of One-Step-Synthesized PEG-Coated Gold Nanoparticles: In Vitro and in Vivo Studies, *Einstein*, 2024, **22**, eAO0764, DOI: **10.31744/einstein_journal/2024AO0764**.

13 J. Omping, R. Unabia, R. L. Reazo, M. Lapening, R. Lumod, A. Ruda, R. B. Rivera, N. L. Sayson, F. Latayada, R. Capangpangan, G. Dumancas, R. Malaluan, A. Lubguban, G. Petalcorin Jr. and A. Alguno, Facile Synthesis of PEGylated Gold Nanoparticles for Enhanced Colorimetric Detection of Histamine, *ACS Omega*, 2024, **9**(12), 14269–14278, DOI: **10.1021/acsomega.3c10050**.

14 M.-C. Daniel and D. Astruc, Gold Nanoparticles: Assembly, Supramolecular Chemistry, Quantum-Size-Related Properties, and Applications toward Biology, Catalysis, and Nanotechnology, *Chem. Rev.*, 2004, **104**(1), 293–346, DOI: **10.1021/cr030698+**.

15 J. Gao, X. Huang, H. Liu, F. Zan and J. Ren, Colloidal Stability of Gold Nanoparticles Modified with Thiol Compounds: Bioconjugation and Application in Cancer Cell Imaging, *Langmuir*, 2012, **28**(9), 4464–4471, DOI: **10.1021/la204289k**.

16 Z. Hou, Z. Wang, R. Liu, H. Li, Z. Zhang, T. Su, J. Yang and H. Liu, The Effect of Phospho-Peptide on the Stability of Gold Nanoparticles and Drug Delivery, *J. Nanobiotechnol.*, 2019, **17**(1), 88, DOI: **10.1186/s12951-019-0522-y**.

17 J. W. Lee, S.-R. Choi and J. H. Heo, Simultaneous Stabilization and Functionalization of Gold Nanoparticles via Biomolecule Conjugation: Progress and Perspectives, *ACS Appl. Mater. Interfaces*, 2021, **13**(36), 42311–42328, DOI: **10.1021/acsami.1c10436**.

18 J. Zong, S. L. Cobb and N. R. Cameron, Peptide-Functionalized Gold Nanoparticles: Versatile Biomaterials for Diagnostic and Therapeutic Applications, *Biomater. Sci.*, 2017, **5**(5), 872–886, DOI: **10.1039/C7BM00006E**.

19 W. A. Arcos Rosero, A. Bueno Barbezan, C. Daruich de Souza and M. E. Chuery Martins Rostelato, Review of Advances in Coating and Functionalization of Gold Nanoparticles: From Theory to Biomedical Application, *Pharmaceutics*, 2024, **16**(2), 255, DOI: **10.3390/pharmaceutics16020255**.

20 R. Daniele, C. Brazzale, B. Arpac, F. Tognetti, C. Pesce, A. Malfanti, E. Sayers, F. Mastrotto, A. T. Jones, S. Salmaso and P. Caliceti, Influence of Folate-Targeted Gold Nanoparticles on Subcellular Localization and Distribution into Lysosomes, *Pharmaceutics*, 2023, **15**(3), 864, DOI: **10.3390/pharmaceutics15030864**.

21 F. Eker, E. Akdaşçi, H. Duman, M. Bechelany and S. Karav, Gold Nanoparticles in Nanomedicine: Unique Properties and Therapeutic Potential, *Nanomaterials*, 2024, **14**(22), 1854, DOI: **10.3390/nano14221854**.

22 D. Drescher, T. Büchner, P. Schrade, H. Traub, S. Werner, P. Guttmann, S. Bachmann and J. Kneipp, Influence of Nuclear Localization Sequences on the Intracellular Fate of Gold Nanoparticles, *ACS Nano*, 2021, **15**(9), 14838–14849, DOI: **10.1021/acsnano.1c04925**.

23 M. R. K. Ali, Y. Wu, D. Ghosh, B. H. Do, K. Chen, M. R. Dawson, N. Fang, T. A. Sulchek and M. A. El-Sayed, Nuclear Membrane-Targeted Gold Nanoparticles Inhibit Cancer Cell Migration and Invasion, *ACS Nano*, 2017, **11**(4), 3716–3726, DOI: **10.1021/acsnano.6b08345**.

24 C. J. Yang and D. B. Chithrani, Nuclear Targeting of Gold Nanoparticles for Improved Therapeutics, *Curr. Top. Med. Chem.*, 2016, **16**(3), 271–280, DOI: **10.2174/1568026615666150701115012**.

25 S. Huo, S. Jin, X. Ma, X. Xue, K. Yang, A. Kumar, P. C. Wang, J. Zhang, Z. Hu and X.-J. Liang, Ultrasmall Gold Nanoparticles as Carriers for Nucleus-Based Gene Therapy Due to Size-Dependent Nuclear Entry, *ACS Nano*, 2014, **8**(6), 5852–5862, DOI: **10.1021/nn5008572**.

26 M. A. Mackey, F. Saira, M. A. Mahmoud and M. A. El-Sayed, Inducing Cancer Cell Death by Targeting Its Nucleus: Solid Gold Nanospheres versus Hollow Gold Nanocages, *Bioconjugate Chem.*, 2013, **24**(6), 897–906, DOI: **10.1021/bc300592d**.

27 J. Yang, A. Griffin, Z. Qiang and J. Ren, Organelle-Targeted Therapies: A Comprehensive Review on System Design for Enabling Precision Oncology, *Signal Transduction Targeted Ther.*, 2022, **7**(1), 1–27, DOI: **10.1038/s41392-022-01243-0**.

28 X. Qin, H. Zhang, X. Xing, P. Wang, J. Yan, D. Liu, Q. Gong, R. Zhang and H. Zhang, Robust Strategies in Nuclear-Targeted Cancer Therapy Based on Functional

Nanomaterials, *Mater. Des.*, 2022, **221**, 110999, DOI: 10.1016/j.matdes.2022.110999.

29 B. Kang, M. A. Mackey and M. A. El-Sayed, Nuclear Targeting of Gold Nanoparticles in Cancer Cells Induces DNA Damage, Causing Cytokinesis Arrest and Apoptosis, *J. Am. Chem. Soc.*, 2010, **132**(5), 1517–1519, DOI: 10.1021/ja9102698.

30 C. S. Bhatt, A. Rajavel, D. S. Parimi, R. N. Sella, J. Murugaiyan and A. K. Suresh, Sustainable Exscalar Monodispersed *Gold* Nanoparticles with Enhanced Dispersion Stability and Biocompatibility for Theragnostics, *ACS Appl. Nano Mater.*, 2023, **6**(13), 12548–12559, DOI: 10.1021/acsanm.3c02407.

31 D.-H. Tsai, M. P. Shelton, F. W. DelRio, S. Elzey, S. Guha, M. R. Zachariah and V. A. Hackley, Quantifying Dithiothreitol Displacement of Functional Ligands from Gold Nanoparticles, *Anal. Bioanal. Chem.*, 2012, **404**(10), 3015–3023, DOI: 10.1007/s00216-012-6418-4.

32 Z. Jin, J. Yeung, J. Zhou, M. Retout, W. Yim, P. Fajtová, B. Gosselin, I. Jabin, G. Bruylants, H. Mattoussi, A. J. O'Donoghue and J. V. Jokerst, Empirical Optimization of Peptide Sequence and Nanoparticle Colloidal Stability: The Impact of Surface Ligands and Implications for Colorimetric Sensing, *ACS Appl. Mater. Interfaces*, 2023, **15**(16), 20483–20494, DOI: 10.1021/acsami.3c00862.

33 O. Olatunji and A. Denloye, Temperature–dependent Extraction Kinetics of Hydrolyzed Collagen from Scales of Croaker Fish Using Thermal Extraction, *Food Sci. Nutr.*, 2017, **5**(5), 1015–1020, DOI: 10.1002/fsn3.488.

34 J. D. Figueroa, S. D. Garcia Schejtman, R. Tu, M. Muñoz, F. Salas-Sepúlveda, H. Poblete, M.-A. Langlois, E. J. Suuronen and E. I. Alarcón, Ultrashort Peptides as Stabilizing Agents for Colloidal Nanogold, *ACS Appl. Mater. Interfaces*, 2025, **17**(14), 21601–21613, DOI: 10.1021/acsami.4c17794.

35 M. Torres-Díaz, C. Abreu-Takemura and L. M. Díaz-Vázquez, Microalgae Peptide-Stabilized Gold Nanoparticles as a Versatile Material for Biomedical Applications, *Life*, 2022, **12**(6), 831, DOI: 10.3390/life12060831.

36 C. D. Walkey and W. C. W. Chan, Understanding and Controlling the Interaction of Nanomaterials with Proteins in a Physiological Environment, *Chem. Soc. Rev.*, 2012, **41**(7), 2780–2799, DOI: 10.1039/C1CS15233E.

37 Ž Krpetić, P. Nativo, F. Porta and M. Brust, A Multidentate Peptide for Stabilization and Facile Bioconjugation of Gold Nanoparticles, *Bioconjugate Chem.*, 2009, **20**(3), 619–624, DOI: 10.1021/bc8003028.

38 J. X. Xu, M. S. Alom, R. Yadav and N. C. Fitzkee, Predicting Protein Function and Orientation on a Gold Nanoparticle Surface Using a Residue-Based Affinity Scale, *Nat. Commun.*, 2022, **13**(1), 7313, DOI: 10.1038/s41467-022-34749-w.

39 M. Ibrahim, E. Ramadan, N. E. Elsadek, S. E. Emam, T. Shimizu, H. Ando, Y. Ishima, O. H. Elgarhy, H. A. Sarhan, A. K. Hussein and T. Ishida, Polyethylene Glycol (PEG): The Nature, Immunogenicity, and Role in the Hypersensitivity of PEGylated Products, *J. Controlled Release*, 2022, **351**, 215–230, DOI: 10.1016/j.jconrel.2022.09.031.

40 Y. Nie, G. Fu and Y. Leng, Nuclear Delivery of Nanoparticle-Based Drug Delivery Systems by Nuclear Localization Signals, *Cells*, 2023, **12**(12), 1637, DOI: 10.3390/cells12121637.

41 W. Wu, Z. Zhou, G. Sun, Y. Liu, A. Zhang and X. Chen, Construction and Characterization of Degradable Fish Scales for Enhancing Cellular Adhesion and Potential Using as Tissue Engineering Scaffolds, *Mater. Sci. Eng. C*, 2021, **122**, 111919, DOI: 10.1016/j.msec.2021.111919.

42 M. Gauza-Włodarczyk, L. Kubisz and D. Włodarczyk, Amino Acid Composition in Determination of Collagen Origin and Assessment of Physical Factors Effects, *Int. J. Biol. Macromol.*, 2017, **104**(Pt A), 987–991, DOI: 10.1016/j.ijbiomac.2017.07.013.

43 M. D. Shoulders and R. T. Raines, Collagen Structure and Stability, *Annu. Rev. Biochem.*, 2009, **78**(Volume 78, 2009), 929–958, DOI: 10.1146/annurev.biochem.77.032207.120833.

44 S. T. Khew, X. H. Zhu and Y. W. Tong, An Integrin-Specific Collagen-Mimetic Peptide Approach for Optimizing Hep3B Liver Cell Adhesion, Proliferation, and Cellular Functions, *Tissue Eng.*, 2007, **13**(10), 2451–2463, DOI: 10.1089/ten.2007.0063.

45 Y. Xu and M. Kirchner, Collagen Mimetic Peptides, *Bioengineering*, 2021, **8**(1), 5, DOI: 10.3390/bioengineering8010005.

46 L. Guerrini, R. A. Alvarez-Puebla and N. Pazos-Perez, Surface Modifications of Nanoparticles for Stability in Biological Fluids, *Materials*, 2018, **11**(7), 1154, DOI: 10.3390/ma11071154.

47 E. Ruoslahti, RGD and other recognition sequences for integrins, *Annu. Rev. Cell Dev. Biol.*, 1996, **12**(Volume 12, 1996), 697–715, DOI: 10.1146/annurev.cellbio.12.1.697.

48 J. Emsley, C. G. Knight, R. W. Farndale, M. J. Barnes and R. C. Liddington, Structural Basis of Collagen Recognition by Integrin Alpha2beta1, *Cell*, 2000, **101**(1), 47–56, DOI: 10.1016/S0092-8674(00)80622-4.

49 A. Roy, C. Pandit, A. Gacem, M. S. Alqahtani, M. Bilal, S. Islam, M. J. Hossain and M. Jameel, Biologically Derived Gold Nanoparticles and Their Applications, *Bioinorg. Chem. Appl.*, 2022, **2022**(1), 8184217, DOI: 10.1155/2022/8184217.

50 M. A. Dobrovolskaia and S. E. McNeil, Immunological Properties of Engineered Nanomaterials, *Nat. Nanotechnol.*, 2007, **2**(8), 469–478, DOI: 10.1038/nnano.2007.223.

51 M. Mahmoudi, I. Lynch, M. R. Ejtehadi, M. P. Monopoli, F. B. Bombelli and S. Laurent, Protein–Nanoparticle Interactions: Opportunities and Challenges, *Chem. Rev.*, 2011, **111**(9), 5610–5637, DOI: 10.1021/cr100440g.

52 M. P. Monopoli, D. Walczyk, A. Campbell, G. Elia, I. Lynch, F. Baldelli Bombelli and K. A. Dawson, Physical–Chemical Aspects of Protein Corona: Relevance to in Vitro and in Vivo Biological Impacts of Nanoparticles, *J. Am. Chem. Soc.*, 2011, **133**(8), 2525–2534, DOI: 10.1021/ja107583h.

53 M. P. Monopoli, C. Åberg, A. Salvati and K. A. Dawson, Biomolecular Coronas Provide the Biological Identity of Nanosized Materials, *Nat. Nanotechnol.*, 2012, **7**(12), 779–786, DOI: **10.1038/nnano.2012.207**.

54 H.-C. Chou, S.-J. Chiu and T.-M. Hu, Quantitative Analysis of Macrophage Uptake and Retention of Fluorescent Organosilica Nanoparticles: Implications for Nanoparticle Delivery and Therapeutics, *ACS Appl. Nano Mater.*, 2024, **7**(4), 3656–3667, DOI: **10.1021/acsanm.3c05058**.

55 P. C. Patel, D. A. Giljohann, W. L. Daniel, D. Zheng, A. E. Prigodich and C. A. Mirkin, Scavenger Receptors Mediate Cellular Uptake of Polyvalent Oligonucleotide-Functionalized Gold Nanoparticles, *Bioconjugate Chem.*, 2010, **21**(12), 2250–2256, DOI: **10.1021/bc1002423**.

56 C. T. Ng, F. M. A. Tang, J. J. Li, C. Ong, L. L. Y. Yung and B. H. Bay, Clathrin-Mediated Endocytosis of Gold Nanoparticles In Vitro, *Anat. Rec.*, 2015, **298**(2), 418–427, DOI: **10.1002/ar.23051**.

57 X. Xie, J. Liao, X. Shao, Q. Li and Y. Lin, The Effect of Shape on Cellular Uptake of Gold Nanoparticles in the Forms of Stars, Rods, and Triangles, *Sci. Rep.*, 2017, **7**(1), 3827, DOI: **10.1038/s41598-017-04229-z**.

58 D. Drescher, T. Büchner, P. Schrade, H. Traub, S. Werner, P. Guttmann, S. Bachmann and J. Kneipp, Influence of Nuclear Localization Sequences on the Intracellular Fate of Gold Nanoparticles, *ACS Nano*, 2021, **15**(9), 14838–14849, DOI: **10.1021/acsnano.1c04925**.

59 Y. Nie, G. Fu and Y. Leng, Nuclear Delivery of Nanoparticle-Based Drug Delivery Systems by Nuclear Localization Signals, *Cells*, 2023, **12**(12), 1637, DOI: **10.3390/cells12121637**.

60 B. D. Chithrani, A. A. Ghazani and W. C. W. Chan, Determining the Size and Shape Dependence of Gold Nanoparticle Uptake into Mammalian Cells, *Nano Lett.*, 2006, **6**(4), 662–668, DOI: **10.1021/nl052396o**.

61 R. Allen and T. Yokota, Endosomal Escape and Nuclear Localization: Critical Barriers for Therapeutic Nucleic Acids, *Molecules*, 2024, **29**(24), 5997, DOI: **10.3390/molecules29245997**.

62 R. Augustine, A. Hasan, R. Primavera, R. J. Wilson, A. S. Thakor and B. D. Kevadiya, Cellular Uptake and Retention of Nanoparticles: Insights on Particle Properties and Interaction with Cellular Components, *Mater. Today Commun.*, 2020, **25**, 101692, DOI: **10.1016/j.mtcomm.2020.101692**.

63 P. Goyal and R. Malviya, Advances in Nuclei Targeted Delivery of Nanoparticles for the Management of Cancer, *Biochim. Biophys. Acta, Rev. Cancer*, 2023, **1878**(3), 188881, DOI: **10.1016/j.bbcan.2023.188881**.

64 D. Drescher, T. Büchner, P. Schrade, H. Traub, S. Werner, P. Guttmann, S. Bachmann and J. Kneipp, Influence of Nuclear Localization Sequences on the Intracellular Fate of Gold Nanoparticles, *ACS Nano*, 2021, **15**(9), 14838–14849, DOI: **10.1021/acsnano.1c04925**.